Arab J Sci Eng (2014) 39:2143–2156
DOI 10.1007/s13369-013-0748-1

RESEARCH ARTICLE - MECHANICAL ENGINEERING

Lattice Boltzmann Simulation of Natural Convection in a Square Cavity with a Linearly Heated Wall Using Nanofluid

GH. R. Kefayati

Received: 1 November 2011 / Accepted: 12 July 2013 / Published online: 5 September 2013

Abstract In this paper, Lattice Boltzmann simulation of natural convection in a square cavity with a linearly heated wall which is filled by nanofluid has been investigated. The fluid in the cavity is a water-based nanofluid containing various nanoparticles such as copper (Cu), cupric oxide (CuO) or alumina (Al_2O_3). This study has been conducted for Rayleigh numbers of 10^3 to 10^5, while solid volume fraction (φ) varied from 0 to 16 %. The effects of nanopartcles are displayed on streamlines, isotherms counters, local and average Nusselt number. Copper nanoparticle enhances heat transfer more than other nanoparticles, while the lowest heat transfer is demonstrated by alumina (Al_2O_3) nanoparticles. In addition, the increment of Rayleigh number causes the effect of the nanoparticles to increase.

Keywords Natural convection · Linearly heated wall · Nanofluid · Lattice Boltzmann method · Heat transfer

الخلاصة

تم - في هذه الورقة - التحقيق في محاكاة بولتزمان الشعرية للحمل الحراري الطبيعي في تجويف مربع مع جدار مسخن خطيا ممتلىء بسائل متناهي الصغر (نانوني). والسائل في التجويف هو سائل نانوني على أساس الماء الذي يحتوي على مختلف جزيئات النحاس (Cu)، وأكسيد النحاس (CuO) أو الألومينا (Al_2O_3) النانوية. وقد أجريت هذه الدراسة على أعداد رايليخ من 10^3 إلى 10^5 في حين أن جزءاً من الحجم الصلب (φ) تغير من 0٪ إلى 16٪. وقد تم عرض آثار الجزيئات النانونية على أعداد التدفقات، وعدادات الأيزوثرم ، وعدد نسلت المحلي والمتوسط. إن جسيمات النحاس النانونية تعزز نقل الحرارة أكثر من غيرها من الجسيمات النانوية في حين يتجلى نقل الحرارة الأقل من قبل جسيمات الألومينا (Al_2O_3) النانوية. بالإضافة إلى ذلك تسبب الزيادة في عدد رايلي زيادة في تأثير الجسيمات النانوية.

List of Symbols

c	Lattice speed
c_i	Discrete particle speeds
c_p	Specific heat at constant pressure
F	External forces
f	Density distribution functions
f^{eq}	Equilibrium density distribution functions
g	Internal energy distribution functions
g^{eq}	Equilibrium internal energy distribution functions
G	Gravity
k	Thermal conductivity
L	Enclosure height
M	Lattice numbers
Ma	Mach number
Nu	Nusselt number
Pr	Prandtl number
R	Constant of the gases
Ra	Rayleigh number
T	Temperature
x, y	Cartesian coordinates

GH. R. Kefayati (✉)
School of Computer Science, Engineering and Mathematics, Flinders University, GPO Box 2100, Adelaide, SA 5001, Australia
e-mail: gh.rkefayati@yahoo.com; gholamrezakefayati@gmail.com; gholamreza.kefayati@flinders.edu.au

Greek letters

ω_i	Weighted factor for flow (D2Q9)
β	Thermal expansion coefficient
φ	Volume fraction
τ_c	Relaxation time for temperature
τ_v	Relaxation time for flow
ρ	Density
μ	Dynamic viscosity
ϑ	Kinematic viscosity
Δx	Lattice spacing
Δt	Time increment
ω_i'	Weighted factor for temperature (D2Q4)

Subscripts

avg	Average
C	Cold
f	Fluid
H	Hot
nf	Nanofluid
s	Solid
*	Normalized

1 Introduction

For more than two decades, Lattice Boltzmann method (LBM) has been demonstrated to be a very effective numerical tool for a broad variety of complex fluid flow phenomena that are problematic for conventional methods [1–17]. The kinetic nature of the LBM distinguishes it from other numerical methods mainly in three aspects. First, the convection operator of the LBM is linear in velocity space, hence computational efforts are greatly reduced as compared to those of some macroscopic CFD methods such as the Navier–Stokes equation solvers. Second, the pressure of the LBM can be directly calculated using an equation of state, unlike the direct numerical simulation of the incompressible Navier–Stokes equations, in which the pressure must be obtained from the Poisson equation. Third, the LBM utilizes a minimal set of velocities in phase space; therefore, the transformation relating the microscopic distribution function and macroscopic quantities is greatly simplified. Analysis of natural convection heat transfer and fluid flow in enclosures has been extensively made using numerical technique experiments for various boundary conditions because of its wide applications and interest in engineering such as nuclear energy, double pane windows, heating and cooling of buildings, solar collectors, electronic cooling, and so on. In this work, this method is used for natural convection in a square cavity with linearly heated wall using nanofluid. Several investigations in natural convection with non-uniformly heated wall have been carried out. Sarris et al. [18] reported the effect of sinusoidal top wall temperature variations in a natural convection within a square cavity where the other walls are insulated. Roy and Basak [19] investigated the influence of uniform and non-uniform heating walls on natural convection flows in a square cavity. Sathiyamoorthy et al. [20] studied natural convection flow in a closed square cavity when the bottom wall is uniformly heated and vertical walls are linearly heated as the top wall is well insulated. An innovative technique to improve heat transfer is using of nanoparticles in the base fluids that have low thermal conductivity such as water [21–30]. Fluids with nanoparticles suspended in them are called nanofluids. Many investigators have studied the flow and thermal characteristics of nanofluids. Khanafer et al. [31] investigated the heat transfer enhancement in a two-dimensional enclosure utilizing nanofluids for various pertinent parameters. They tested different models for nanofluid density, viscosity, and thermal expansion coefficients. It was found that the suspended nanoparticles substantially increase the heat transfer rate at any given Grashof numbers. Putra et al. [32] conducted the experiment for observation on the natural convective characteristics of water based on alumina (Al_2O_3). They reported that natural convective heat transfer in a cavity is decreased with the increment of the volume fraction of nanoparticles. Hwang et al. [33] studied thermal characteristics of natural convection in a rectangular cavity heated from below with water-based nanofluids containing alumina (Al_2O_3). They theoretically investigated with Jang and Choi's model for predicting the effective thermal conductivity of nanofluids and various models for the effective viscosity. They showed that the ratio of heat transfer coefficient of nanofluids to the base fluid is decreased as the size of nanoparticles increases, or the average temperature of nanofluids is decreased. Santra et al. [34] studied the effect of copper–water nanofluid as a cooling medium to simulate the behavior of heat transfer due to laminar natural convection in a differentially heated square cavity. They obtained that the heat transfer plunged with the augmentation of volume fraction for a particular Rayleigh number, while it enhances with Rayleigh number for a particular volume fraction. Oztop and Abu-Nada [35] researched heat transfer and fluid flow due to buoyancy forces in a partially heated enclosure using nanofluids. They found that both increasing the value of Rayleigh number and heater size enhances the heat transfer and flow strength, keeping other parameters fixed. Moreover, they exhibited that heat transfer rises with enhancement of the value of volume fraction of nanoparticles.

Abu-Nada et al. [36] investigated heat transfer enhancement in horizontal annuli using nanofluids. Jahanshahi et al. [37] numerically investigated the effects due to uncertainties in effective thermal conductivity according to experimental and theoretical formulations of the SiO_2–water nanofluid on laminar natural convection heat transfer in a square enclosure. Recently, scientists have strived to solve nanofluids

in different shapes and boundary conditions because of its widespread applications [38–43]. Kefayati et al. [44] utilized this method (LBM) for simulating natural convection in tall enclosures using water/ SiO_2 nanofluid. They obtained that the average Nusselt number increases with volume fraction for the whole range of Rayleigh numbers and aspect ratios and the effect of nanoparticles on heat transfer augments as the enclosure aspect ratio increases.

The aim of the present paper is to the study effect of a linearly heated wall on flow field and temperature distribution in nanofluid-filled enclosure. Furthermore, it is demonstrated to present the ability of LBM for solving problems of nanofluid in various boundary conditions. The results of the method are validated with previous numerical investigations. Influences of all parameters (Rayleigh number, volume fraction, and different nanoparticles) on flow field and temperature distribution are considered.

2 Mathematical Formulation

2.1 Problem Statement

The geometry of the present problem is shown in Fig. 1. It displays a two-dimensional enclosure with the height of L. The temperature of the enclosure right wall is maintained at (T_C), while the left wall has a constant temperature profile of ($T_H(y) = T_H - (T_H - T_C)y/L$). The top horizontal wall has been considered to be adiabatic, while the bottom wall has a constant temperature (T_H). Thermophysical properties of the nanofluids are assumed to be constant (Table 1). The density variation in the nanofluids is approximated by the standard Boussinesq model. The enclosure is filled with a mixture of water and solid nanoparticles. The nanofluid is assumed to be Newtonian, incompressible, and laminar. In addition, it is considered while the liquid and solid nanoparticles are in thermal equilibrium and equal velocity.

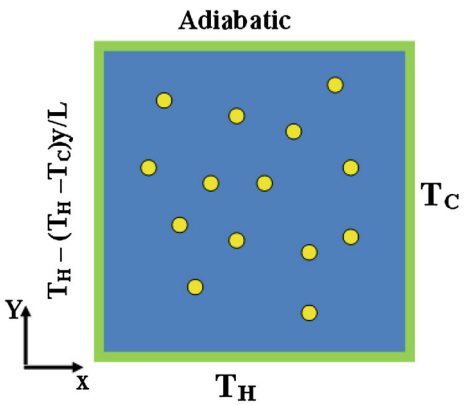

Fig. 1 Geometry of the present study

Table 1 Thermophysical properties of water and nanoparticles

Property	Fluid phase (water)	Solid phase (Cu)	Solid phase (Cuo)	Solid phase (Al_2O_3)
C_p (J/Kg k)	4,179	383	540	765
ρ (kg/m^3)	997.1	8,954	6,500	3,970
k (W/m K)	0.6	400	18	25
β (K^{-1})	2.1E−4	1.67E−6	8.5E−6	8.5E−6
α (m^2/s)	1.44E−7	–	–	–
μ (kg/ms)	8.9E−4	–	–	–

2.2 Lattice Boltzmann Method

For the incompressible problems, LBM utilizes two distribution functions, f and g, for the flow and temperature fields, respectively [13].

For the flow field:

$$f_i(x + c_i\Delta t, t + \Delta t) - f_i(x, t) = -\frac{1}{\tau_v}\left[f_i(x, t) - f_i^{eq}(x, t)\right] + \Delta t F_i \quad (1)$$

For the temperature field:

$$g_i(x + c_i\Delta t, t + \Delta t) - g_i(x, t) = -\frac{1}{\tau_c}\left[g_i(x, t) - g_i^{eq}(x, t)\right] \quad (2)$$

where the discrete particle velocity vectors defined c_i (Fig. 2), Δt denotes lattice time step which is set to unity. τ_v and τ_c are the relaxation time for the flow and temperature fields, respectively. f_i^{eq} and g_i^{eq} are the local equilibrium distribution functions that have an appropriately prescribed functional dependence on the local hydrodynamic properties which are calculated with Eqs. (3) and (4) for flow and temperature fields, respectively. Also F is an external force term.

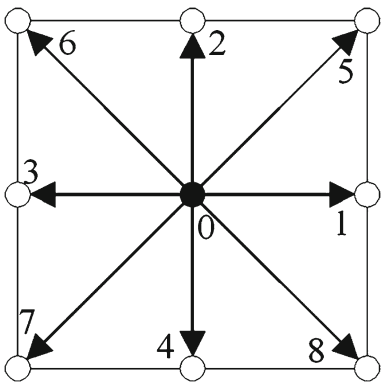

Fig. 2 The discrete velocity vectors for D2Q9

$$f_i^{\mathrm{eq}}(x,t) = \omega_i \rho \left[1 + 3\frac{c_i u}{c^2} + \frac{9}{2}\frac{(c_i u)^2}{c^4} - \frac{3}{2}\frac{uu}{c^2}\right] \tag{3}$$

$$g_i^{\mathrm{eq}} = \omega_i' T \left[1 + 3\frac{c_i u}{c^2}\right] \tag{4}$$

u and ρ are the macroscopic velocity and density, respectively, c is the lattice speed and equals to $\Delta x/\Delta t$ where Δx is lattice space and similar to lattice time step is equal to unity, ω_i is the weighting factor for flow, ω_i' is the weighting factor for temperature.

D2Q9 model for flow, and D2Q4 model for temperature are used in this work, thus the weighting factors and the discrete particle velocity vectors are different for these two models and they are calculated as follows:

For D2Q9

$$\omega_i = \begin{cases} 4/9 & i = 0 \\ 1/9 & i = 1-4 \\ 1/36 & i = 5-8 \end{cases} \tag{5}$$

The discrete velocities, c_i, for the D2Q9 (Fig. 2) are defined as follows:

$$c_i = \begin{cases} 0 & i = 0 \\ c(\cos[(i-1)\pi/2], \sin[(i-1)\pi/2]) & i = 1-4 \\ c\sqrt{2}(\cos[(i-5)\pi/2+\pi/4], \sin[(i-5)\pi/2+\pi/4]) & i = 5-8 \end{cases} \tag{6}$$

For D2Q4

The weighting factor for temperature is equal for each main four directions which is $\omega_i' = 0.25$.

The discrete velocities, c_i, for the D2Q4 are defined as follows:

$$c_i = \left(\cos\left(\frac{i-1}{2}\pi\right), \sin\left(\frac{i-1}{2}\pi\right)\right)c \quad i = 1-4 \tag{7}$$

The kinematic viscosity (υ) and the thermal diffusivity (α) are then related to the relaxation times by:

$$\vartheta = \left[\tau_{\mathrm{v}} - \frac{1}{2}\right]c_{\mathrm{s}}^2 \Delta t \quad \text{and} \quad \alpha = \left[\tau_{\mathrm{c}} - \frac{1}{2}\right]c_{\mathrm{s}}^2 \Delta t \tag{8}$$

where c_{s} is the lattice speed of sound in media, it is equal to $c/\sqrt{3}$.

In the simulation, the Boussinessq approximation is applied to the buoyancy force term; therefore, the force term is determined by:

$$F = \rho G \beta \Delta T \tag{9}$$

where G is the gravitational vector, ΔT is the temperature difference that it is equal to $(T - T_{\mathrm{m}})$ as $T_{\mathrm{m}} = \frac{T_{\mathrm{H}}+T_{\mathrm{c}}}{2}$ and β is the thermal expansion coefficient.

The force term added to the collision process in Eq. (1) is given by [13]:

$$F_i \omega_i \; F \cdot c_i / c_{\mathrm{s}}^2 \tag{10}$$

Finally, the macroscopic quantities (ρ, u, T) can be calculated by the mentioned variables, with the following formula.

$$\text{Flowdensity: } \rho(x,t) = \sum_i f_i(x,t) \tag{11}$$

$$\text{Momentum: } \rho u(x,t) = \sum_i f_i(x,t) c_i \tag{12}$$

$$\text{Temperature: } T = \sum_i g_i(x,t) \tag{13}$$

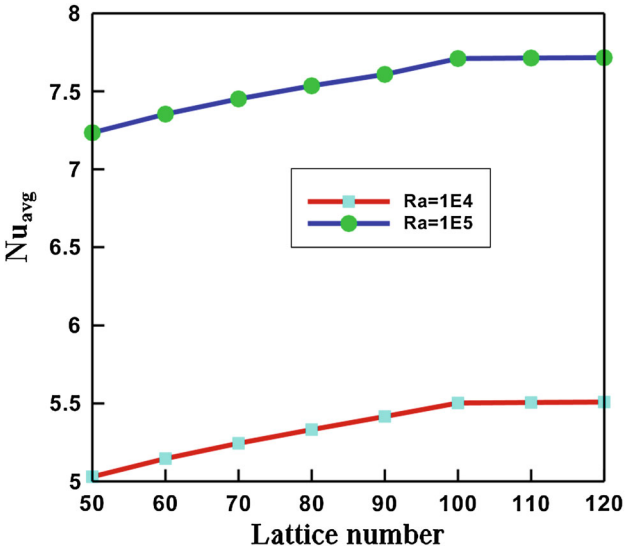

Fig. 3 Grid independent test ($\varphi = 0.04$)

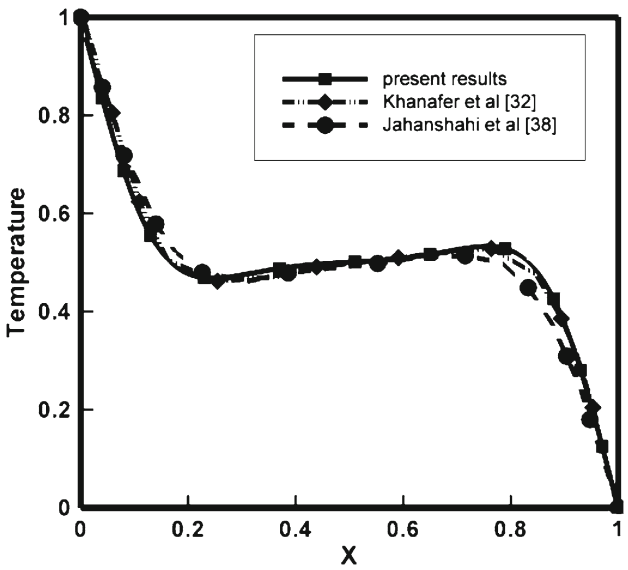

Fig. 4 Comparison of the temperature at the middle of the cavity between the present results and numerical results by Khanafer et al. [31] and Jahanshahi et al. [37] ($Pr = 6.2$, $\varphi = 0.1$, $Gr = 10^4$)

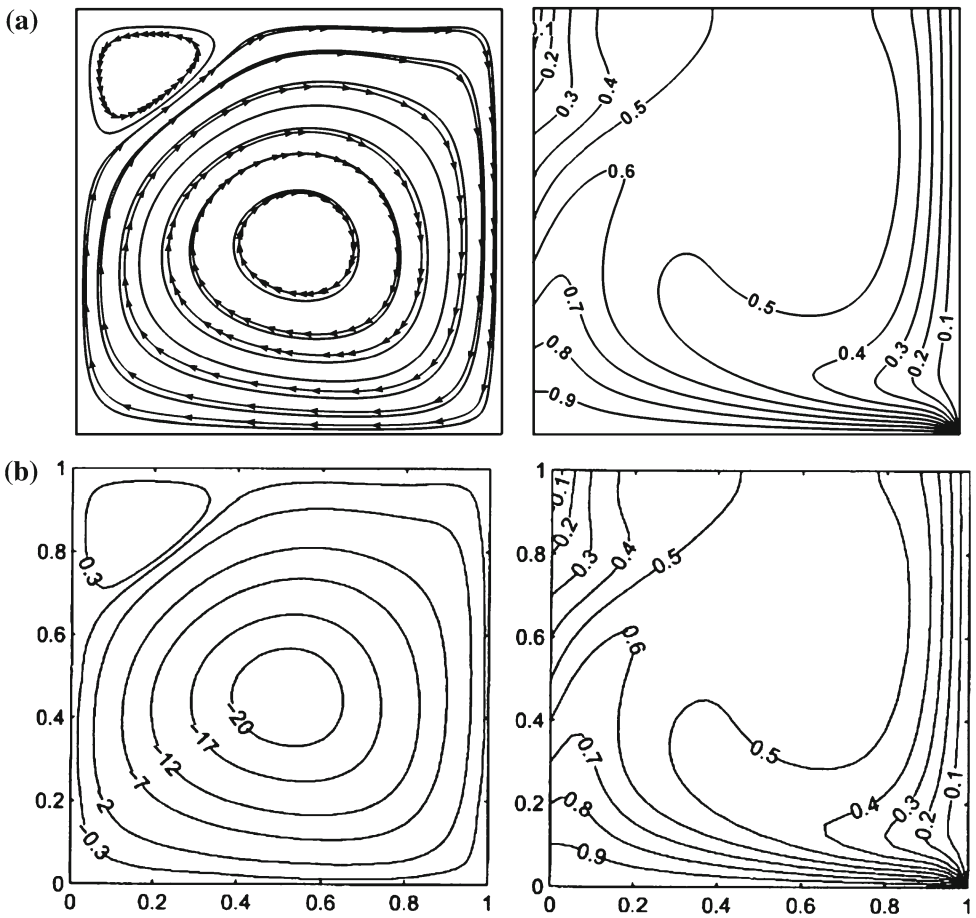

Fig. 5 Comparison of the streamlines and isotherms at $Ra = 10^5$ between **a** the present results and **b** numerical results by Sathiyamoorty et al. [20]

2.3 Boundary Conditions

2.3.1 Flow

Bounce-back boundary conditions were applied on all solid boundaries, which mean that incoming boundary populations are equal to out-going populations after the collision [12]. For instance, for the east boundary, the following conditions are imposed:

$$f_{6,n} = f_{8,n}, \qquad f_{7,n} = f_{5,n}, \qquad f_{4,n} = f_{2,n} \tag{14}$$

where n is the lattice number on the boundary.

2.3.2 Temperature

Bounce-back boundary condition (adiabatic) is used on the north of the boundaries. For example, the north boundary, the following condition is imposed:

$$g_{4,n} = g_{2,n}$$

Temperature at the west, east, and bottom walls are known, in the west wall $T_{\mathrm{H}}(y) = T_{\mathrm{H}} - (T_{\mathrm{H}} - T_{\mathrm{C}})y/L$. Since we are using D2Q4, the unknown is g_1 which is evaluated as:

$$g_1 = T_H(y)(\omega_1 + \omega_3) - g_3. \tag{15}$$

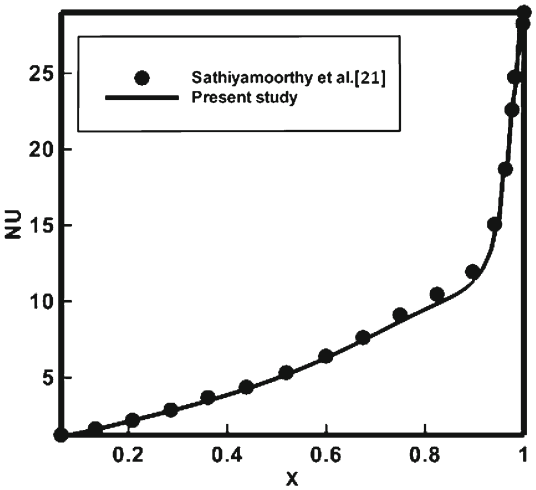

Fig. 6 Comparison of the Nusselt number distribution at $Ra = 10^5$ between the present results and numerical results by Sathiyamoorthy et al. [20]

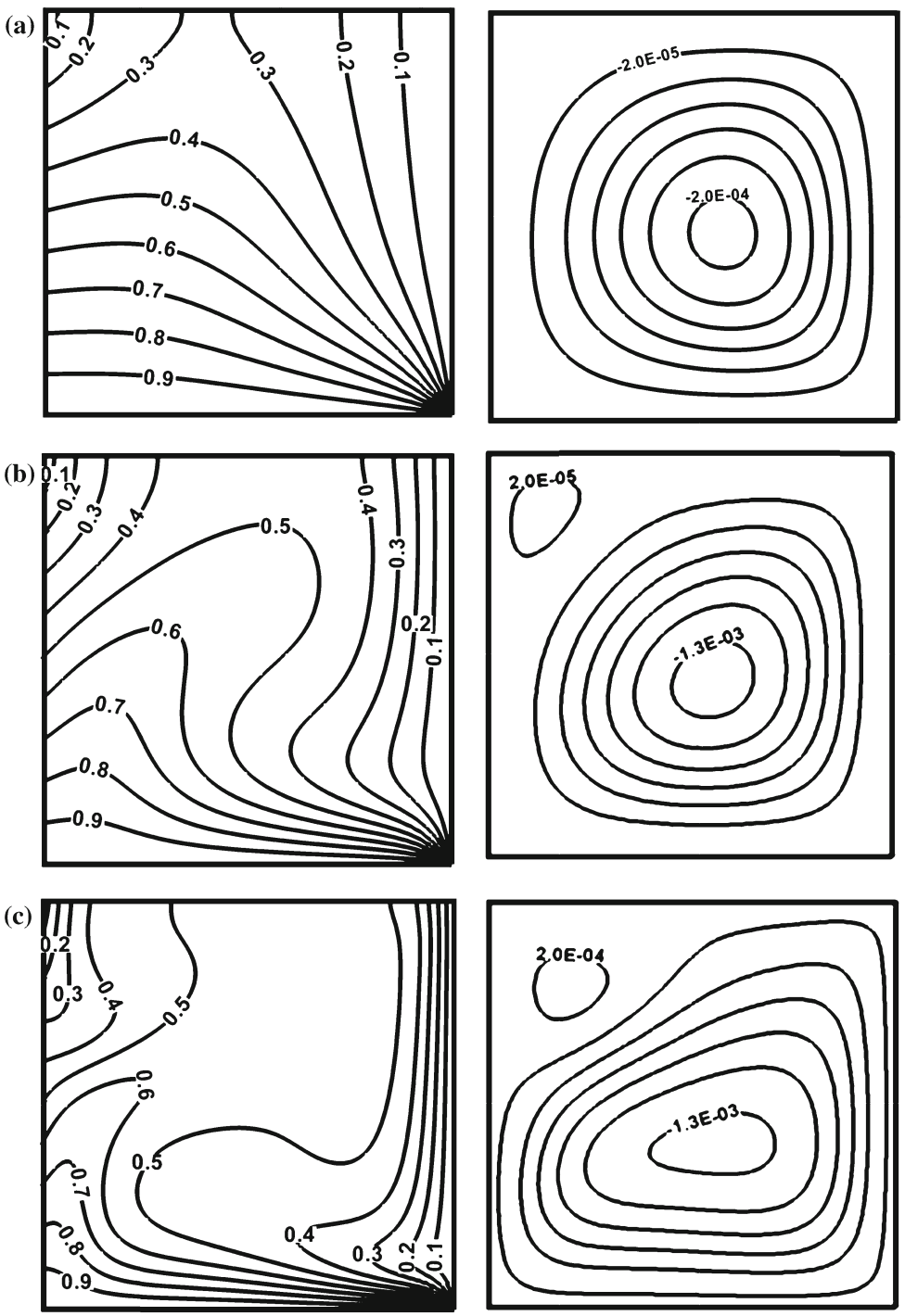

Fig. 7 Comparison of the streamlines and isotherms at $\varphi = 0$ for various Rayleigh numbers **a** $Ra = 10^3$, **b** $Ra = 10^4$, **c** $Ra = 10^5$

2.4 Method of Solution

By fixing Rayleigh number, Prandtl number and Mach number, the viscosity and thermal diffusivity are calculated from the definition of these:

$$\vartheta = \sqrt{\frac{Ma^2 M^2 Prc^2}{Ra}} \tag{16}$$

where M is number of lattices in y-direction (parallel to gravitational acceleration). Rayleigh and Prandtl numbers are defined as $Ra = \frac{\beta g M^3 (T_H - T_C)}{\vartheta \alpha}$, and $Pr = \frac{\vartheta}{\alpha}$, respectively. Besides, the speed of the lattice is constant $\left(c = \frac{1}{\sqrt{3}}\right)$. Mach number was fixed at $Ma = 0.1$ in the present study. After defining the whole parameters of Eq. (16), we can get viscosity and subsequently thermal diffusivity. Finally, Eq. (8)

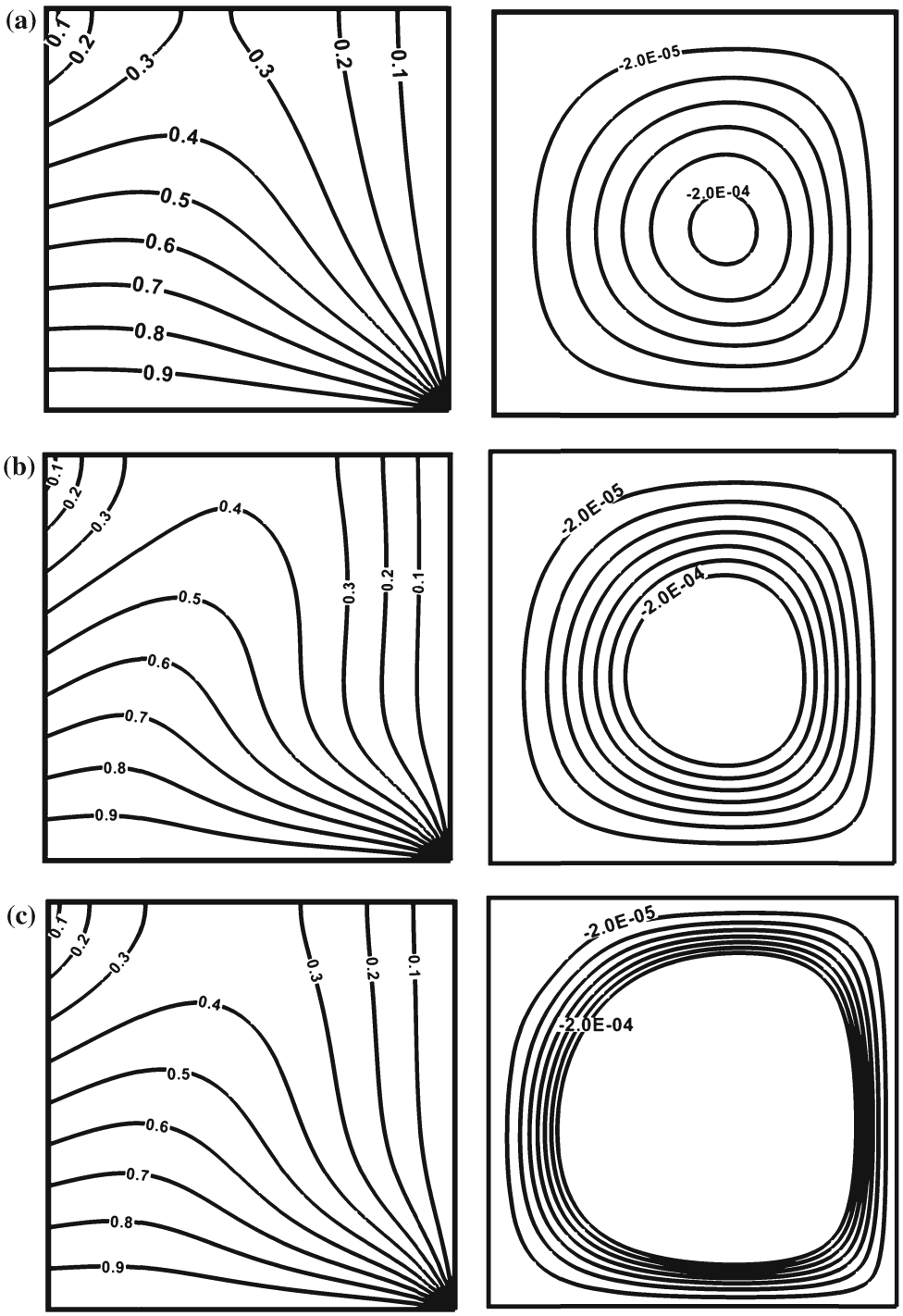

Fig. 8 Comparison of the streamlines and isotherms at $Ra = 10^3$ for different volume fractions of copper/water nanofluid **a** $\varphi = 0$, **b** $\varphi = 0.04$, **c** $\varphi = 0.08$, **d** $\varphi = 0.12$, **e** $\varphi = 0.16$

is used to calculate the relaxation times for density and temperature distribution functions.

2.5 Lattice Boltzmann Method for Nanofluid

The major control parameter of the test case is the Rayleigh number, $Ra = \frac{\beta g_y H^3 Pr(T_H - T_C)}{\vartheta^2}$ with $Pr = \frac{\mu c_p}{k}$ where the parameters have altered with the characters of nanofluid. In fact, the nanofluids were assumed to be similar to a pure fluid and then nanofluid qualities were obtained from Eqs. 17 to 21, applying in the Rayleigh and Prandtl numbers. The pertinent thermophysical properties are given in Table 1.

The effective density of a nanofluid is given by [23]:

$$\rho_{nf} = (1 - \varphi)\rho_f + \varphi\rho_s \tag{17}$$

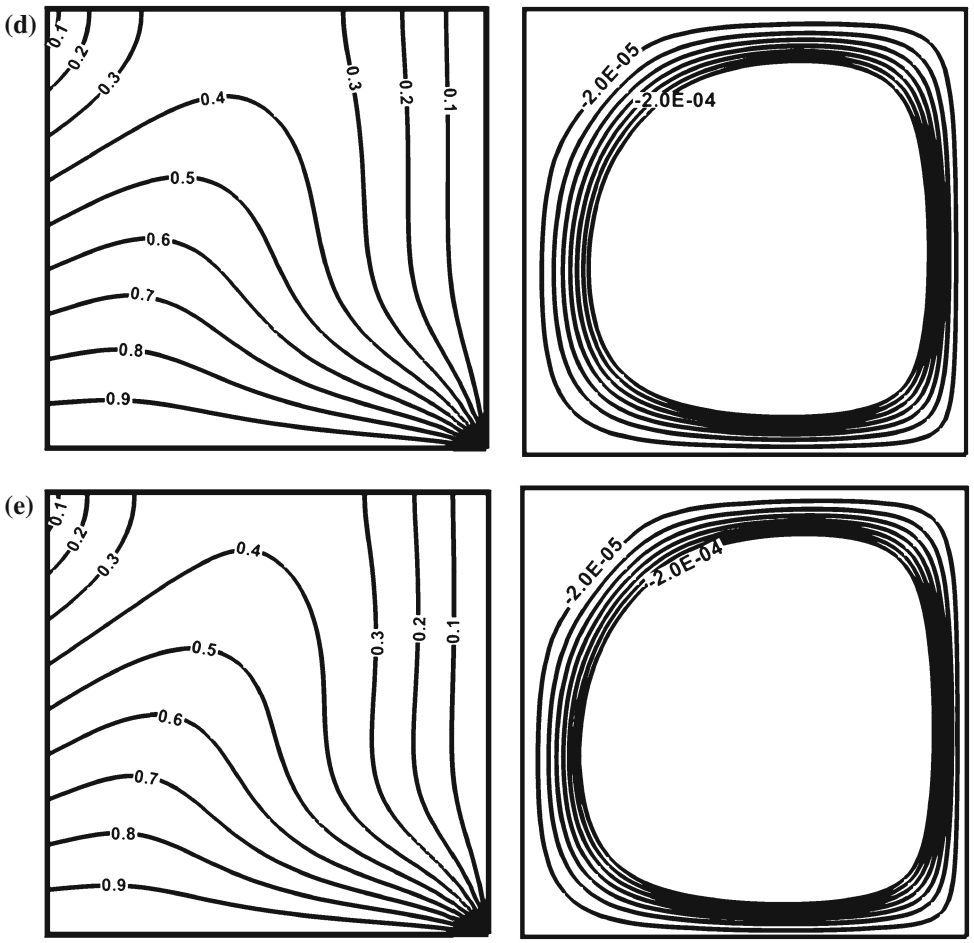

Fig. 8 continued

whereas the heat capacitance of the nanofluid and part of the Boussinesq term are [25]:

$$(\rho c_{\mathrm{p}})_{\mathrm{nf}} = (1-\varphi)(\rho c_{\mathrm{p}})_{\mathrm{f}} + \varphi(\rho c_{\mathrm{p}})_{\mathrm{s}} \tag{18}$$

$$(\rho\beta)_{\mathrm{nf}} = (1-\varphi)(\rho\beta)_{\mathrm{f}} + \varphi(\rho\beta)_{\mathrm{s}} \tag{19}$$

where φ is being the volume fraction of the solid particles, subscripts f, nf and s stand for base fluid, nanofluid and solid, respectively. The viscosity of the nanofluid containing a dilute suspension of small rigid spherical particles is given by [28]:

$$\mu_{\mathrm{nf}} = \frac{\mu_{\mathrm{f}}}{(1-\varphi)^{2.5}} \tag{20}$$

The effective thermal conductivity of the nanofluid can be approximated by the Maxwell-Garnetts (MG) model where the nanoparticles are assumed to be the same and have spherical shapes [25]:

$$\frac{k_{\mathrm{nf}}}{k_{\mathrm{f}}} = \frac{k_{\mathrm{s}} + 2k_{\mathrm{f}} + 2\varphi(kf - ks)}{k_{\mathrm{s}} + 2k_{\mathrm{f}} - \varphi(k_{\mathrm{f}} - k_{\mathrm{s}})} \tag{21}$$

Nusselt number Nu is one of the most important dimensionless parameters in the description of the convective heat transport. The Nusselt number is used as an indicator of heat transfer enhancement where an increase in Nusselt number corresponds to enhancement in heat transfer.

The local Nusselt number and the average value on the walls are calculated as:

$$Nu_y = -\frac{L}{\Delta T}\frac{\partial T}{\partial x} \tag{22}$$

$$Nu_{\mathrm{avg}} = \frac{1}{L}\int_0^L Nu_y \, d_y. \tag{23}$$

Because of the convenience, a normalized average Nusselt number is defined as the ratio of Nusselt number at any volume fraction of nanoparticles to that of pure water, that is as follows:

$$^{*}Nu_{\mathrm{avg}}(\varphi) = \frac{Nu_{\mathrm{avg}}(\varphi)}{Nu_{\mathrm{avg}}(\varphi = 0)} \tag{24}$$

Finally, the stream function is defined in the usual way as:

$$u = \frac{\partial \psi}{\partial y} \quad v = -\frac{\partial \psi}{\partial x} \tag{25}$$

It is taken that $\psi = 0$ at all walls of the cavity.

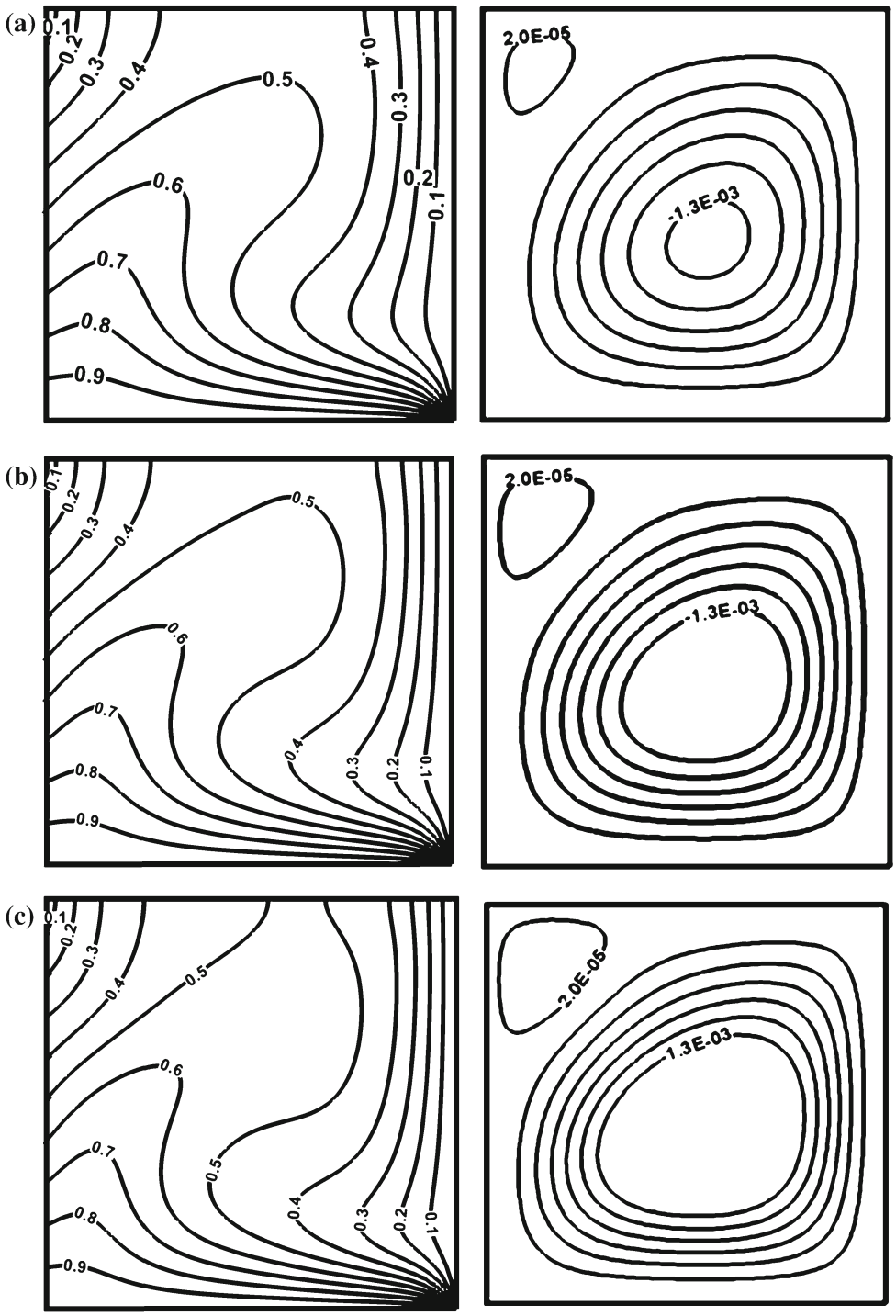

Fig. 9 Comparison of the streamlines and isotherms at $Ra = 10^4$ for different volume fractions of copper/water nanofluid **a** $\varphi = 0$, **b** $\varphi = 0.04$, **c** $\varphi = 0.08$, **d** $\varphi = 0.12$, **e** $\varphi = 0.16$

3 Code Validation and Grid Independence

This problem was investigated at different Rayleigh numbers of 10^3, 10^4, and 10^5, and five different volume fractions of $\varphi = 0.0, 0.04, 0.08, 0.12$ and 0.16 for various nanoparticles of Cu, CuO, and Al_2O_3. LBM scheme was used for obtaining the numerical simulations in a cavity with a linearly heated wall that is filled from nanofluid of water/Cu. An extensive mesh testing procedure was conducted to guarantee a grid independent solution. Eight different mesh combinations were explored for the case of $\varphi = 0.04$. The present code was tested for grid independence by calculating the average Nusselt number on the bottom wall. In harmony with this, it was found that a grid size of 101×101 ensures a grid independent solution. It was confirmed that the grid size (101×101) ensures a grid independent solution as portrayed

Fig. 9 continued

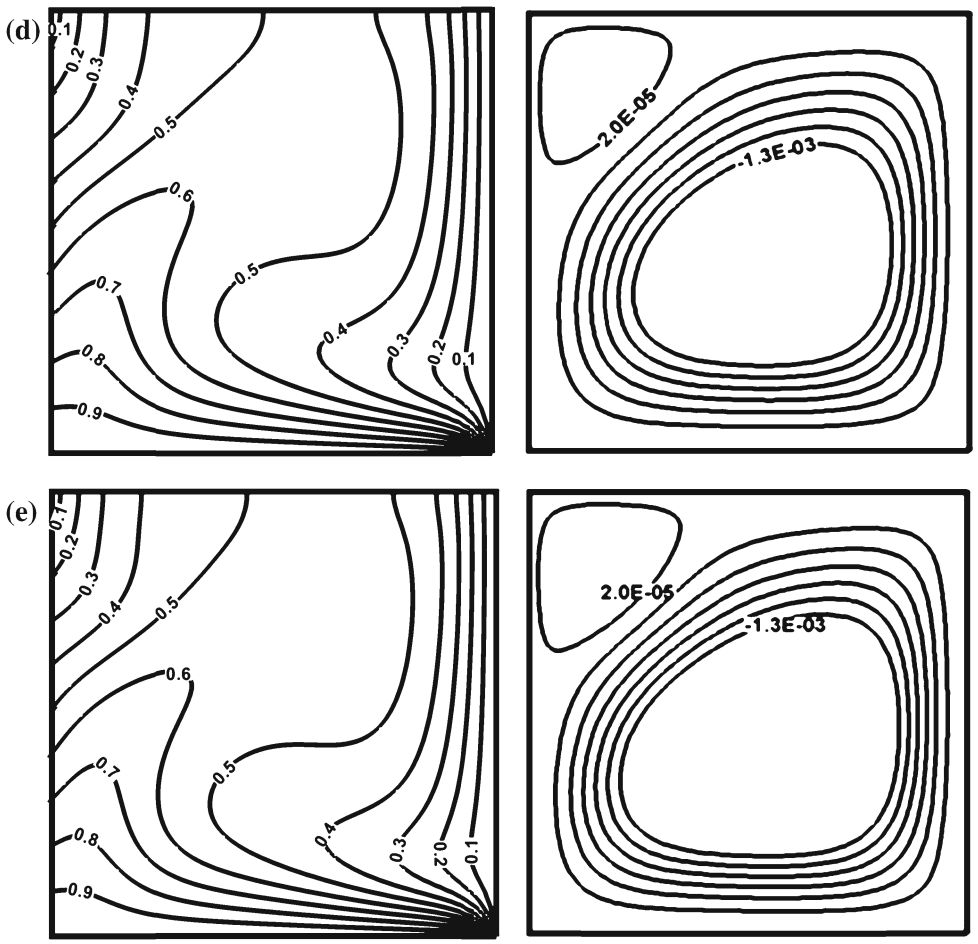

by Fig. 3. The method of solution for nanofluid by LBM was validated against results of Khanafer et al. [31] and Jahanshahi et al. [37] where the middle temperature of the cavity for nanoparticle of Cu at $\varphi = 0.1$ was investigated (Fig. 4). Moreover, in this code was utilized the method of kefayati et al. [43,44] for nanofluid as they demonstrated the ability of LBM for simulating of nanofluids in the articles. To check the accuracy of the present results, the present code is validated against published work in the literature on a cavity with a linearly heated wall, while it was filled by air with $Pr = 0.71$ and $Ra = 10^5$ [20]. The results are compared in Fig. 5 as the streamlines and isotherms have a good agreement between both compared methods. Figure 6 demonstrates Nusselt number distribution on the bottom wall of the cavity at $Ra = 10^5$, $Pr = 0.7$ against the numerical simulation of Sathiyamoorthy et al. [20].

4 Result and Discussion

4.1 Effect of Rayleigh Number on Streamlines and Isotherms

Figure 7 displays the stream function and the isotherm contours at $Ra = 10^3$, 10^4 and 10^5 for pure water. At $Ra = 10^3$, the isotherms move from the left wall linearly and smoothly, but the isotherms gather at the bottom corner of the cavity right wall as they near the right wall of the cavity. When Rayleigh number increases, the isotherms rise up toward the top wall of the cavity and change intensely. Furthermore, the isotherms near the bottom wall of the cavity. It causes the gradient of the isotherms to increase which eventuate to enhance heat transfer in this region. At $Ra = 10^3$, the stream lines form clockwise inside the cavity where a weak circulation is obtained at the left corner of the cavity upper counterclockwise as Rayleigh number augments. This secondary circulation is formed due to the improvement of convection process. Moreover, the values of two circulations enhance as Rayleigh number rises. At $Ra = 10^5$, the stream lines traverse more distance within the cavity and near the walls that the phenomena provokes the boundary layer thickness to plummet and eventually heat transfer increases.

4.2 Effect of Nanoparticle Volume Fraction on Streamlines and Isotherms

Figure 8 illustrates the stream lines and the isotherm contours for various volume fractions at $Ra = 10^3$. Most changes in the isotherms are observed from $\varphi = 0$ to 0.08 where

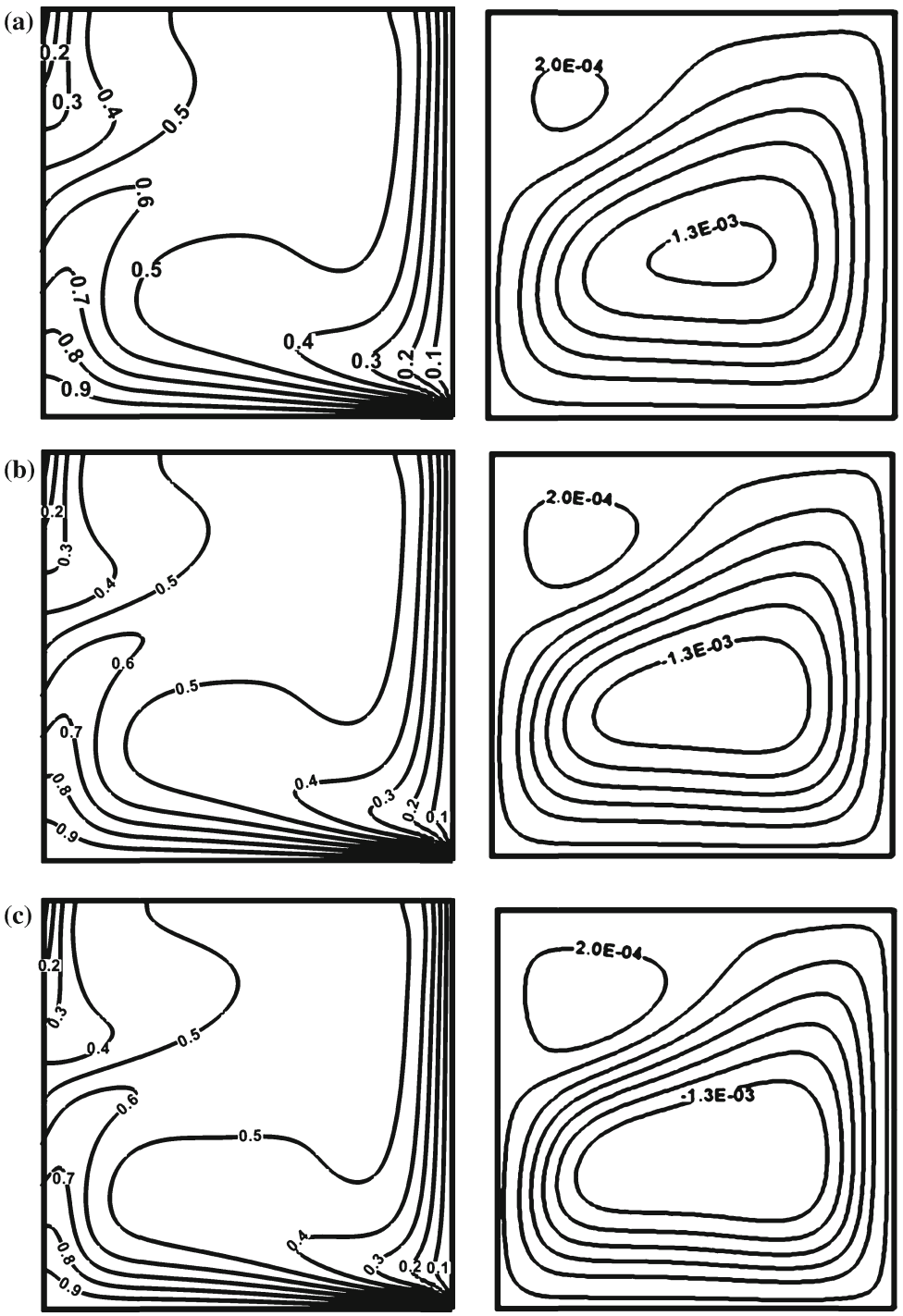

Fig. 10 Comparison of the streamlines and isotherms at $Ra = 10^5$ for different volume fractions of copper/water nanofluid **a** $\varphi = 0$, **b** $\varphi = 0.04$, **c** $\varphi = 0.08$, **d** $\varphi = 0.12$, **e** $\varphi = 0.16$

the isotherm of $T = 0.3$ moves to the upper of the cavity completely and shows that the gradient of the isotherm on the hot bottom wall enhances which causes heat transfer to increase. We followed a certain value of the streamlines for different volume fractions in the streamlines. It is obvious that the core of the streamline expands when the volume fractions enhance for the specific values of stream functions.

Figure 9 exhibits the streamlines and the isotherms at $Ra = 10^4$, as the volume fraction alters from 0 to 0.16. The isotherm of $T = 0.5$ moves to the upper of the cavity and the gradient of the isotherms in the upper section of the cavity left wall increases. Moreover, the compression of the isotherms near the bottom wall augments with the growth of the volume fractions. The weak circulation in the upper section of the cavity left wall ameliorates and occupies more

Fig. 10 continued

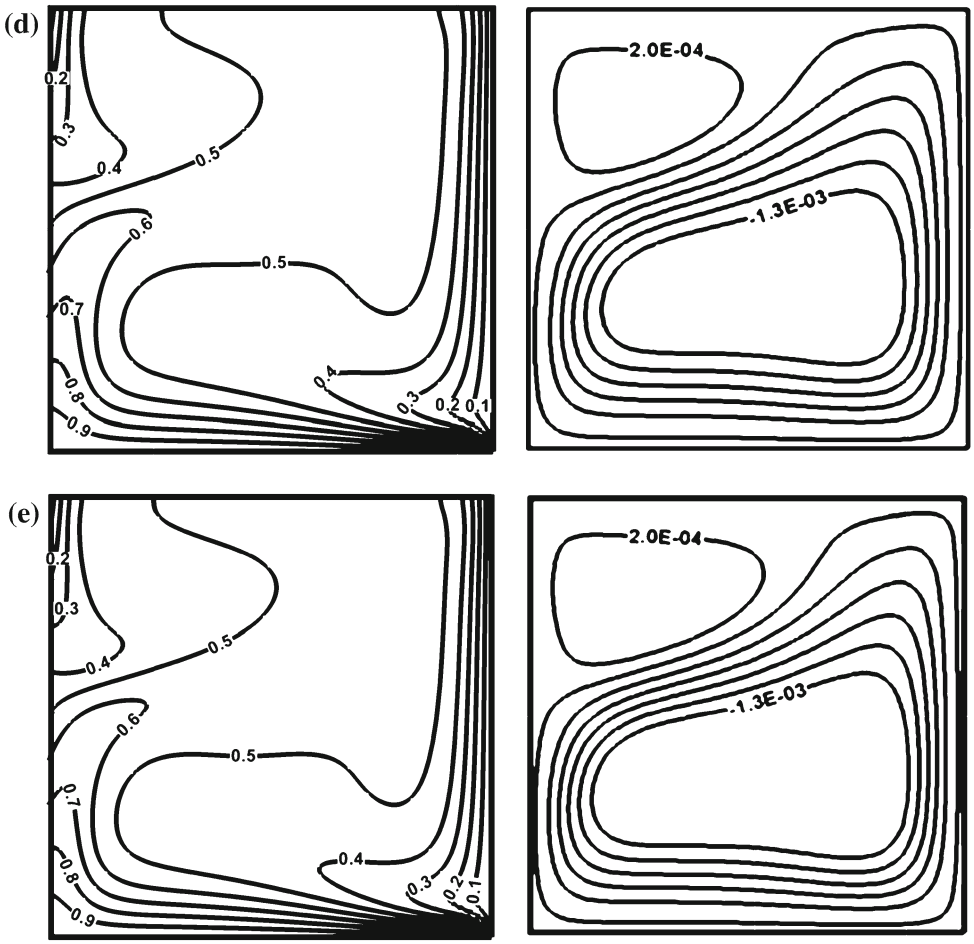

spaces within the cavity when the volume fraction enhances. It is clear for a certain value of the streamlines that both circulations expand with the rise of the volume fractions.

Figure 10 shows the effect of the increment of the volume fraction on the streamlines and the isotherms. The isotherms are influenced by the volume fractions marginally and the most changes can be observed from $\varphi = 0$ to 0.04, but the effect of nanoparticles is immensely considerable on the streamlines where the streamlines shape elliptically. This new form of the streamlines helps the convection process improve in the cavity.

4.3 Effect of Rayleigh Number and Various Nanofluids on Average Nusselt Number

Figure 11 depicts the variation of the normalized Nusselt number (NU^*_{avg}) on the hot bottom wall of the cavity toward the volume fraction of copper nanoparticles for different Rayleigh numbers. It illustrates that NU^*_{avg} augments with the enhancement of the volume fraction for different Rayleigh numbers. In addition, it demonstrates that NU^*_{avg} increases as Rayleigh number enhances. These results demonstrate the effects of nanoparticles on heat transfer grow with the augmentation of Rayleigh number as the normalized Nusselt number has the least value for various volume fractions at $Ra = 10^3$.

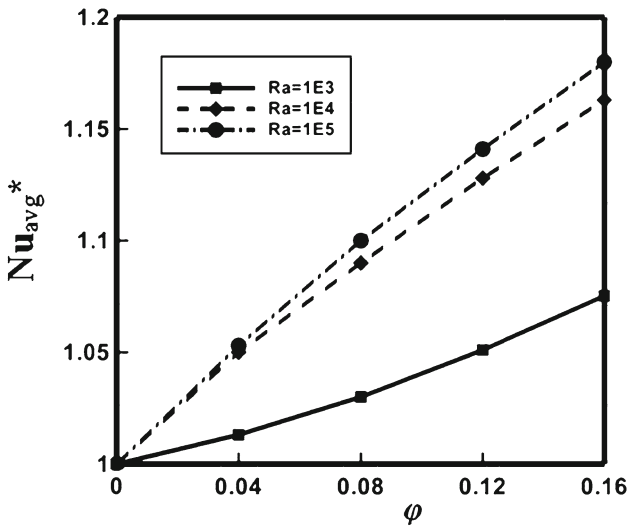

Fig. 11 Values of the normalized average Nuseelt number at different volume fractions and various Rayleigh numbers for copper/water nanofluid

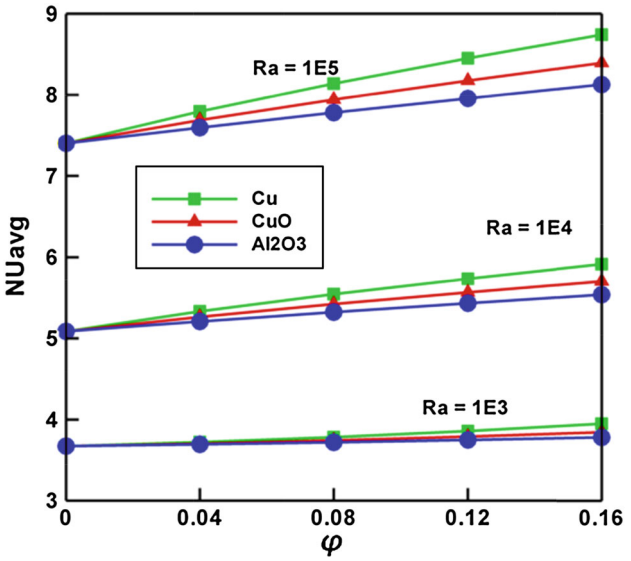

Fig. 12 Values of the average Nusselt numbers at different volume fractions, nanoparticles and Rayleigh numbers

Figure 12 displays the average Nusselt number on the hot bottom wall of the cavity at various nanoparticles and the volume fractions of nanofluid with different Rayleigh numbers. It shows that the average Nusselt number increases with a similar trend for various nanoparticles at different Rayleigh numbers, but the enhancement is different for multifarious nanoparticles. For instance, at $Ra = 10^5$, the average Nusselt number augments by 17.56 % for Cu, 12.16 % for CuO and 8 % for Al_2O_3. Furthermore, the highest and the lowest average Nusselt numbers are obtained as Cu and Al_2O_3 nanoparticles are used, respectively.

5 Conclusions

Natural convection in a cavity with a linearly heated wall which is filled with water as the base fluid and three different nanoparticles of Cu, CuO, and Al_2O_3 have been conducted numerically by LBM. This study has been carried out for the pertinent parameters in the following ranges: the Rayleigh number of base fluid, $Ra = 10^3 - 10^5$, the volume fractions 0–16 % and some conclusions were summarized as follows:

(a) A proper validation with previous numerical investigations demonstrates that LBM is an appropriate method for multiphase flow problems with different boundary conditions.
(b) Generally, the increase in the volume fractions and the Rayleigh numbers result in the augmentation of heat transfer.
(c) The effect of nanoparticles on heat transfer augments as Rayleigh number increases as the growth is marginal from $Ra = 10^4$ to 10^5.
(d) The nanoparticles of Cu demonstrate the best effect on heat transfer among other nanoparticles.
(e) The nanoparticles increment causes the streamlines to expand and the secondary circulation at $Ra = 10^4$ and 10^5 occupies more space within the cavity.

References

1. Chen, S.; Doolen, G.: Lattice Boltzmann method for fluid flows. Annu. Rev. Fluid Mech. **30**, 329–364 (1998)
2. Alexander, F.J.; Chen, S.; Sterling, J.D.: Lattice Boltzmann thermohydrodynamics. Phys. Rev. E **47**, 2249–2252 (1993)
3. Qian, Y.: Simulating thermohydrodynamics with lattice BGK models. J. Sci. Comput. **8**, 231–241 (1993)
4. Chen, Y.; Ohashi, H.; Akiyama, M.: Thermal lattice Bhatnagar–Gross–Krook model without nonlinear deviations in macrodynamic equations. Phys. Rev. E **50**, 2776 –2783 (1994)
5. Bartoloni, A.; Battista, C.: LBE simulations of Rayleigh–Bernard convection on the APE100 parallel processor. Int. J. Modul. Phys. C **4**, 993–1006 (1993)
6. Eggles, G.J.M.; Somers, J.A.: Numerical simulation of free convective flow using the lattice-Boltzmann scheme. Int. J. Heat Fluid Flow **16**, 357–364 (1995)
7. Shan, X.: Simulation of Rayleigh–Bernard convection using a lattice-Boltzmann method. Phys. Rev. E **55**, 2780–2788 (1997)
8. Filippova, O.; Hanel, D.: A novel BGK approach for low Mach number combustion. J. Comput. Phys. **158**, 139–160 (2000)
9. Mei, R.; Shyy, W.; Yu, D.; Luo, L.S.: Lattice Boltzmann method for 3-D flows with curved boundary. J. Comput. Phys. **161**, 680–699 (2000)
10. Succi, S.: The Lattice Boltzmann Equation for Fluid Dynamics and Beyond. Clarendon Press, Oxford, London (2001)
11. Mohamad, A.A.: Applied Lattice Boltzmann Method for Transport Phenomena, Momentum, Heat and Mass Transfer. Sure, Calgary (2007)
12. Aghajani, D.M.; Farhadi, M.; Sedighi, K.: Effect of discrete heater at the vertical wall of the cavity over the heat transfer and entropy generation using LBM. Thermal Sci. **14**, 469–477 (2010)
13. Mohamad, A.A.; Kuzmin, A.: A critical evaluation of force term in lattice Boltzmann method, natural convection problem. Int. J. Heat Mass Transf. **53**, 990–996 (2010)
14. Mohamad, A.A.; Bennacer, R.; El-Ganaoui, M.: Double dispersion, natural convection in an open end cavity simulation via Lattice Boltzmann Method. Int. J. Thermal Sci. **49**, 1944–1953 (2010)
15. Mussa, M.A.; Abdullah, S.; Nor Azwadi, C.S.; Muhamad, N.: Simulation of natural convection heat transfer in an enclosure by the lattice-Boltzmann method. Comp. Fluids **44**, 162–168 (2011)
16. Sajjadi, H.; Gorji, M.; Kefayati, GH.R.; Ganji, D.D.: Lattice Boltzmann simulation of MHD mixed convection in two sided lid-driven square cavity. Heat Transf. Asian Res. **41**(2), 179–195 (2012)
17. Sajjadi, H.; Gorji, M.; Hosseinizadeh, S.F.; Kefayati, GH.R.; Ganji, D.D.: Numerical analysis of turbulent natural convection in square cavity using large-Eddy simulation in Lattice Boltzmann method. Iran J. Sci. Tech. Trans. B/Eng. **35**, 133–142 (2011)
18. Sarris, I.E.; Lekakis, I.; Vlachos, N.S.: Natural convection in a 2D enclosure with sinusoidal upper wall temperature. Numer. Heat Transf. Part A **42**, 513–530 (2002)
19. Roy, S.; Basak, T.: Finite element analysis of natural convection flows in a square cavity with nonuniformly heated wall(s). Int. J. Eng. Sci. **43**, 668–680 (2005)

20. Sathiyamoorthy, M.; Basak, T.; Roy, S.; Pop, I.: Steady natural convection flows in a square cavity with linearly heated side wall(s). Int. J. Heat Mass Transf. **50**, 766–775 (2007)
21. Choi, U.S.: Enhancing thermal conductivity of fluids with nanoparticles. ASME Fluids Eng. Div. **231**, 99–105 (1995)
22. Lee, S.; Choi, S.U.S.; Li, S.; Eastman, J.A.: Measuring thermal conductivity of fluids containing oxide nanoparticles. ASME J. Heat Trans. **121**, 280–289 (1999)
23. Eastman, J.A.; Choi, S.U.S.; Yu, W.; Thompson, L.J.: Anomalously increased effective thermal conductivity of ethylene glycol-based nanofluids containing copper nanoparticles. Appl. Phys. Lett. **78**, 718–720 (2001)
24. Das, S.K.; Putra, N.; Thiesen, P.; Roetzel, W.: Temperature dependence of thermal conductivity enhancement for nanofluids. ASME J. Heat Transf. **125**, 567–574 (2003)
25. Jang, S.P.; Choi, S.U.S.: The role of Brownian motion in the enhanced thermal conductivity of nanofluids. Appl. Phys. Lett. **84**, 4316–4318 (2004)
26. Das, S.K.; Putra, N.; Roetzel, W.: Pool boiling characteristics of nanofluids. Int. J. Heat Mass Transf. **46**, 851–862 (2003)
27. Yang, Y.; Zhang, Z.G.; Grulke, E.A.; Anderson, W.B.; Wu, G.: Heat transfer properties of nanoparticle-in-fluid dispersions (nanofluids) in laminar flow. Int. J. Heat Mass Transf. **48**, 1107–1116 (2005)
28. Xuan, Y.; Li, Q.: Investigation on convective heat transfer and flow features of nanofluids. ASME Trans. J. Heat Transf. **125**, 151–155 (2003)
29. Wen, D.; Ding, Y.: Experimental investigation into convective heat transfer of nanofluid at the entrance region under laminar flow conditions. Int. J. Heat Mass Transf. **47**, 5181–5188 (2004)
30. Heris, S.Z.; Etemad, S.G.; Esfahany, M.N.: Experimental investigation of oxide nanofluids laminar flow convective heat transfer. Int. Commun. Heat Mass **33**, 529–535 (2006)
31. Khanafer, K.; Vafai, K.; Lightstone, M.: Buoyancy-driven heat transfer enhancement in a two-dimensional enclosure utilizing nanofluids. Int. J. Heat Mass Transf. **46**, 3639–3653 (2003)
32. Putra, N.; Roetzel, W.; Das, S.K.: Natural convection of nanofluids. Int. J. Heat Mass Transf. **39**, 775–784 (2003)
33. Hwang, K.S.; Lee, J.-H.; Jang, S.P.: Buoyancy-driven heat transfer of water-based Al_2O_3 nanofluids in a rectangular cavity. Int. J. Heat Mass Transf. **50**, 4003–4010 (2007)
34. Santra, A.K.; Sen, S.; Chakraborty, N.: Study of heat transfer augmentation in a differentially heated square cavity using copper–water nanofluid. Int. J. Thermal Sci. **47**, 1113–1122 (2008)
35. Oztop, H.F.; Abu-Nada, E.: Numerical study of natural convection in partially heated rectangular enclosures filled with nanofluids. Int. J. Heat Fluid Flow **29**, 1326–1336 (2008)
36. Abu-Nada, E.; Masoud, Z.; Hijazi, A.: Natural convection heat transfer enhancement in horizontal concentric annuli using nanofluids. Int. Commun. Heat Mass Transf. **35**(5), 657–665 (2008)
37. Jahanshahi, M.; Hosseinizadeh, S.F.; Alipanah, M.; Dehghani, A.; Vakilinejad, G.R.: Numerical simulation of free convection based on experimental measured conductivity in a square cavity using water/SiO_2 nanofluid. Int. Commun. Heat Mass Transf. **37**, 687–694 (2010)
38. Moraveji, K.M.; Darabi, M.; Haddad, S.M.H.; Davarnejad, R.: Modeling of convective heat transfer of a nanofluid in the developing region of tube flow with computational fluid dynamics. Int. Commun. Heat Mass Transf. **38**, 1291–1295 (2011)
39. Mahmoodi, M.; Hashemi, S.M.: Numerical study of natural convection of a nanofluid in C-shaped enclosures. Int. J. Thermal Sci. **55**, 76–89 (2012)
40. Mahmoodi, M.: Numerical simulation of free convection of a nanofluid in L-shaped cavities, Int. J. Thermal Sci. **50**, 1731–1740 (2011)
41. Arefmanesh, A.; Amini, M.; Mahmoodi, M.; Najafi, M.: Buoyancy-driven heat transfer analysis in two-square duct annuli filled with a nanofluid. European J. Mech. B/Fluids **33**, 95–104 (2012)
42. Mahmoodi, M.: Numerical simulation of free convection of nanofluid in a square cavity with an inside heater. Int. J. Thermal Sci. **50**, 2161–2175 (2011)
43. Kefayati, GH.R.; Hosseinizadeh, S.F.; Gorji, M.; Sajjadi, H.: Lattice Boltzmann simulation of natural convection in an open enclosure subjugated to water/copper nanofluid, Int. J. Thermal Sci. **52**, 91–101 (2012)
44. Kefayati, GH.R.; Hosseinizadeh, S.F.; Gorji, M.; Sajjadi, H.: Lattice Boltzmann simulation of natural convection in tall enclosures using water/ SiO_2 nanofluid. Int. Commun. Heat Mass Transf. **38**, 798–80 (2011)